Exploring the limits of a Leica DM EP microscope and Anlysing image enhancement techniques

TU Delft, Faculty of Applied Sciences,
BSc program Applied Physics

Delft, March 30th 2020
van Loon, Reinaart
Sangers, Jeroen

Abstract

In this report the reader will be informed about the experiments performed for the Microscopy research project.

For the experiments a Leice DM EP polarising microscope in combination with a CCD camera was used to determine the magnification of the microscope with three objectives, the width of a human hair and optical fibre, the resolving power for multiple different numerical apertures, the cross section of elliptical starch particles and the birefringence of an unknown crystal. Finally, an image of a fungus sample will be improved by using different python algorithms.
The magnification and resolving power of the microscope with the objectives, the width of a human hair and optical fibre and the cross section of starch particles were found by making images using the CCD camera and counting pixels. This yielded the following results: For the magnification we found pixel lengths equal to $1.5 \cdot 10^{-6}$, $6.4 \cdot 10^{-7}$ and $1.6 \cdot 10^{-7}$ for the $4\times$, $10\times$ and $40\times$ objectives respectively. For the width of a human hair and optical fibre; diameters of $d_{hair} = 6.57 \pm 0.08 \cdot 10^{-5}$ and $d_{fibre} = 1.26 \pm 0.01 \cdot 10^{-4}$ meters were found. The mean cross section of elliptical starch particles was found to be $A_{starch} = 1.9 \cdot 10^{-10}\ m^2$ with a standard deviation $\sigma = 8 \cdot 10^{-11}\ m^2$. The size measurements yielded results that matched literature. However, the measurements on the starch particles turned out to be inadequate given the shape and number of unresolvable particles.
Determining the birefringence of the crystal was done by placing the crystal between to polarising filters and then measuring the difference in height between two colour planes, using this thickness and the colour of the plane, a birefringence number of $\Delta n = 5.3 \pm 0.2 \cdot 10^{-2}$ was found. Therefore, the crystal could either be astrophylite, silk or piemontite. Given that there is an unidentified measurement error, the validity of the outcome is debatable.
Improving the image of a fungus sample, using the sigmoid function and a contrast enhancing rank filter works well, significantly improving the contrast. A bilateral mean filter proves to be of use when removing noise. It does however, remove some of the details. A morphological contrast enhancement filter can be useful for size measurements or line detection. Combination of the different rank filters also seems to be useful to either reveal much detail or to remove noise, compensated by gain of contrast.

Contents

1 Introduction

Microscopes are used extensively in natural sciences. They enable us to image small objects and structures which cannot be resolved by the human eye. The use of microscopes, could for example, aid in studies of biological cells, molecular structures or object classification. To correctly conduct such microscopy studies, it is vital to know what the possibilities and limits are using a particular microscope are in combination with image improvement techniques.

This experiment will focus on a Leica DM EP polarising microscope in combination with a colour CCD and to what extent this set-up can be used to measure the size of small objects and find the birefringence of an unknown crystal. Furthermore, the possibilities of digital image improvement will be investigated.

After calibrating the pixels and finding the resolving power with the aid of a microscopic ruler and resolution target, images are made of a human hair, an optical fibre, starch particles, an unknown birefringent crystal and a fungus sample.

To find the size of the human hair, fibre and particles, computer techniques will be used. The birefringence of the crystal will be determined by focussing on the differently coloured planes of the crystal. Using this to find the thickness of each colour plane and its colour, the birefringence can be calculated. Finally some python algorithms are implemented on the image of the fungus to investigate improvements on contrast and noise reduction. These algorithms are a sigmoid function and the bilateral mean, contrast enhancing and morphological contrast enhancing filters from the rank Sci-kit package.

In section 2 the theory regarding the experiment will be described, followed by the experimental method in section 3. The results and discussion can be found in section 4. Lastly the conclusions in section 5.

2 Theory

A polarising microscope is used for the experiments in this report. In this section the basic principles of a polarising microscope and the theory that is used for the experiments are described.

2.1 Microscopy

Most modern microscopes are compound microscopes which can achieve a relatively high angular magnification for nearby objects ([1]). See figure 1 for a schematic drawing of a basic compound microscope.
Polarising microscopes are a type of microscopes that make use of polarising windows. A polariser is placed in between the light source and the sample and an analyser is placed after the sample. Since the polariser and analyser block all the light except for one specific light polarisation, they allow the viewer to see some of the sample's optical properties such as birefringence.

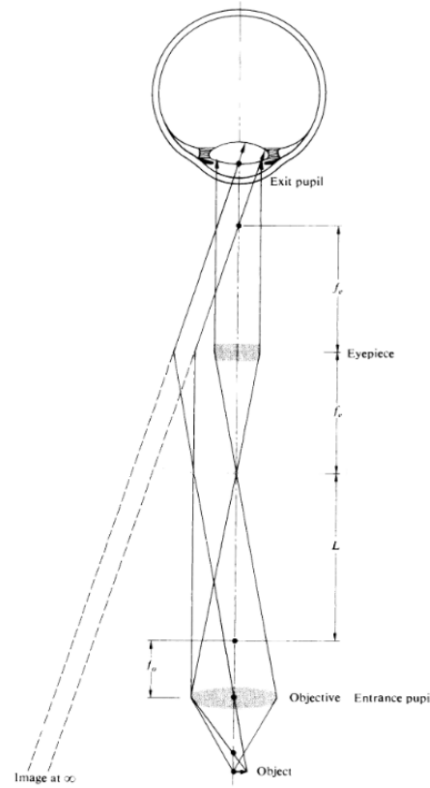

Figure 1: Schematic drawing of a compound microscope. f_e and f_o correspond to respectively to the focussing distance of the eyepiece and objective. This figure was apdapted from Hecht, 2016 [1].

2.2 size measurements

In this experiment a CCD camera was used to record the images from the microscope. To measure distances in a sample it is possible to convert a distance in pixels, n_{pixels}, to physical units such as meters. For this, we need a conversion factor that gives the length in meters per pixel, l_{pixel}. The physical distance, $d_{physical}$ can easily be calculated using equation 1. The value for l_{pixel} should be larger for greater magnifying power.

$$d_{physical} = l_{pixel} \cdot n_{pixels} \tag{1}$$

One of the purposes of this experiment is to find out whether it is possible to do microscopic measurements with the given microscope. Human hairs and glass fibres have a diameter in the range of 10 - 100 μm. Measuring the diameter could give insights into the suitability of the given microscope for measurements of this scale.
Another purpose for a microscope could be to find sizes of many particles. From this information one could get the average particle size and the distribution for these values. Starch particles have a size up to 100 μm and are often ellipse-shaped ([2]). The size of ellipse-shaped starch particles will be measured in this experiment. The cross section of a particle, A, can be calculated using the major and minor diameter of the ellipse, respectively a and b, and equation 2.

$$A = \frac{a \cdot b \cdot \pi}{4} \tag{2}$$

2.3 Birefringence

Birefringence is an optical property that arises when the refractive index depends on the polarization of incoming light. The quantity birefringence, Δn, is characterized as the maximum difference between the two refractive indices for differently polarised light ([1]).

When a birefringent material is viewed in a polarising microscope with the polariser and analyser crossed, bright colours may be observed. The polarised light entering the sample can be decomposed into two orthogonal components, which will experience a different refractive index due to the birefringent property. The difference in refractive index is result in a path length difference, Δl_{path}, between the two orthogonal components. When these two components interfere, the sum of the two might have changed polarisation direction, allowing the light to pass the analyser. A schematic diagram of this process can be seen in figure 2.

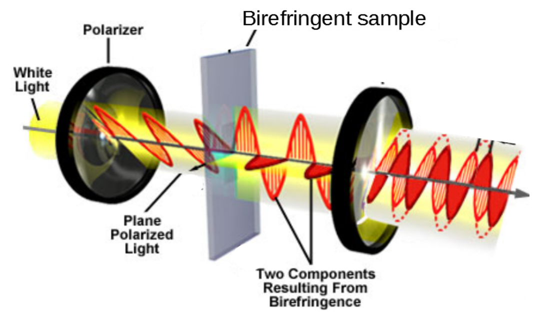

Figure 2: Schematic diagram of birefringence between two crossed polarizing windows. This figure was adapted from Olympus, 2012 [3].

Δl_{path} depends on the thickness of the sample, D, but also on the wavelength of the light ([1]). This means that, for a specific thickness of the sample, the sample will result in positive interference for one wavelength and (partially) negative interference for the others. Subsequently, one colour will be observed for a specific sample thickness. A colour on a Michel-Lévy colour chart ([4]) corresponds to a value for Δl_{path}. Subsequently, the value for Δn can be determined using equation (3) ([1]).

$$\Delta l_{path} = D \cdot \Delta n \tag{3}$$

2.4 Computerised image improvement

One of the goals of the experiment is to devise and test digital filters to improve image quality, by icreasing contrast and removing unwanted noise.
Image features are easier to distinguish when the contrast is high. A way of quantitatively expressing image contrast is through a histogram as outlined in the NI Vision article [5]. As illustrated by the two greyscale images in figure 3 and 4, the high contrast image in figure 3, has pixel intensity peaks that are spread over the whole intensity range compared to the peaks of figure 4. The features of figure 3 are therefore easier to resolve than the features in figure 4. One way to improve contrast is by applying a contrast improving function on the pixel values of an image. This function will work by spreading these intensity peaks further apart on the spectrum.

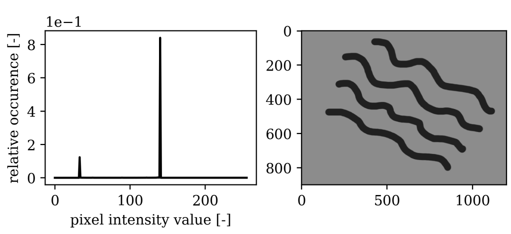

Figure 3: High contrast photo

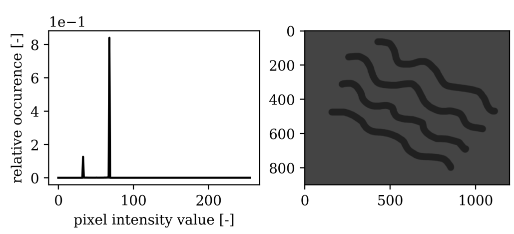

Figure 4: Low contrast photo

Noise is a phenomenon that cannot be evaded. However, some of the noise can be removed by using digital filters, such as rank, median and NxN filters ([6]).
Some images suffer from unwanted information, such as uneven illumination or shot noise. Some of this can easily be removed since they only occur in another frequency-domain than the information we are interested in. One way to select only wanted frequencies is by using Fourier transformations. In this experiment, the sigmoid function to improve contrast and rank filters from the python Sci-kit package are studied and to what extend they can be used to improve an image.

2.5 Error calculation

If Y is a variable which is a function of A,B,C, ... Then the error of Y, $u(Y)$, is given by equation 4.

$$u(Y) = \sqrt{\left(u(A)\frac{\partial Y}{\partial A}\right)^2 + \left(u(B)\frac{\partial Y}{\partial B}\right)^2 + \left(u(C)\frac{\partial Y}{\partial C}\right)^2 + ...} \tag{4}$$

From this it follows that $u(d_{physical})$, $u(A)$ and $u(\Delta n)$, are given respectively by equations 5, 6 and 7.

$$u(d_{physical}) = \sqrt{\left(u(l_{pixel}) \cdot n_{pixels}\right)^2 + \left(u(n_{pixels}) \cdot l_{pixel}\right)^2} \tag{5}$$

$$u(A) = 1/4 \cdot \pi \sqrt{(u(a) \cdot b)^2 + (u(b) \cdot a)^2} \tag{6}$$

$$u(\Delta n) = \sqrt{\left(u(\Delta l_{path}) \cdot \frac{1}{D}\right)^2 + \left(u(D) \cdot \frac{\Delta l_{path}}{D^2}\right)^2} \tag{7}$$

3 Experimental method

This experiment consists of four parts. At first the calibration of the microscope. Secondly size measurements of respectively a human hair, an optical glass fibre and starch particles. Thirdly determining the birefringence of an unknown crystal and finally the computerised improvement of an image of a biological fungus sample. The different experimental methods will be treated separately.

The microscope that is used in all experiments is a Leica DM EP microscope. Its manual can be found in appendix Appendix A. This microscope is used in combination with 4×, 10×, 40× Hi Plan POL objectives with respectively a 0.10, a 0.22 and a 0.65 numerical aperture. A color CCD camera in combination with NI Vision Assistant software is used to acquire digital images.

3.1 Calibration

A microscopic ruler is used to measure the length that corresponds to one pixel in an image, l_{pixel}. This is achieved by focussing on a 1 mm, 100 division ruler and measuring the distance between two focussed, distant division lines and comparing the number of pixels to the physical length. The NI software is used to find the exact location of these two lines and subsequently find the perpendicular projection distance, n_{pixels}. This procedure is repeated for all three objectives.

With the aid of a 1951 USAF resolution target, the resolving power of each objective can be found by first taking a focussed gray-scale image of the target and then taking a perpendicular intensity profile for each well defined three-bar structure (see Figure 6). This intensity profile is exported by NI Vision to a CSV file directly so we dont suffer from any compression losses, a file which can be easily read by a python peakfinding script (an example of which can be seen in the next section's figure 7). The high and low intensity values will be used to calculate the visibility using equation 8 will be plotted along with the corresponding spatial frequency. This is repeated for all three objectives.

$$V = \frac{I_{max} - I_{min}}{I_{max} + I_{min}} \tag{8}$$

3.2 Microscopic size measurements

All microscopic size measurements are made by measuring pixels and comparing this to the corresponding pixel length. This is done for images with the 40× objective since this gives the smallest error.

Human hair and optical glass fibre

Measuring the thickness of the human hair and optical glass fibre is done with the aid of the NI Vision software. First finding the two straight lines of the outer edges and subsequently measuring the perpendicular distance between the two, n_{hair} and n_{gf}, in pixels. The physical size, d_{hair} and d_{gf}, and error can be calculated using equation 1 and 5.

Starch particles

In order to measure the size of individual starch particles, a small amount of starch is mixed with oil. Images are taken at different locations in the mixture. For ellipse-shaped particles that are focussed in the image, an ellipse can be fitted manually. Using the values for the major and minor axis, respectively a and b, the estimated errors and equations 2 and 6, the area of the ellipse, A, and corresponding error can be calculated.

For this experiment it was chosen to find the ellipse size for 30 particles.

3.3 Birefringence

In order to find the birefringence, Δn, of the unknown crystal, it is placed in the microscope with the polariser crossed with respect to the analyser. The crystal is then turned until bright colours can be seen. Now the difference in path length, Δl_{path}, is measured as a function of the thickness, D, of the crystal. D can be found by viewing a border between adjacent colour planes and subsequently noting the focussed position, f, of each colour plane. Taking the difference between two values of f will give the difference in thickness, Δd, between two colour planes. Simple addition and subtraction will give the values for D. The bottom of the sample (black) is also to be taken into account with the same procedure as described above. The birefringence can subsequently be found using orthogonal distance regression with equation 3 and the acquired data.

For this experiment it was chosen to find D and Δl_{path} for 5 colour planes. The focussing process was repeated 4 to 5 times for every border that was studied.

3.4 Image improvement methods

A sigmoid function is a function $f(x)$ that maps its domain to values between zero and one. This sigmoid equation 9 depends on two parameters α and β which respectively define the center and the width of the function as in [7].

$$f(x) = \frac{1}{1 + e^{-\frac{x-\alpha}{\beta}}} \tag{9}$$

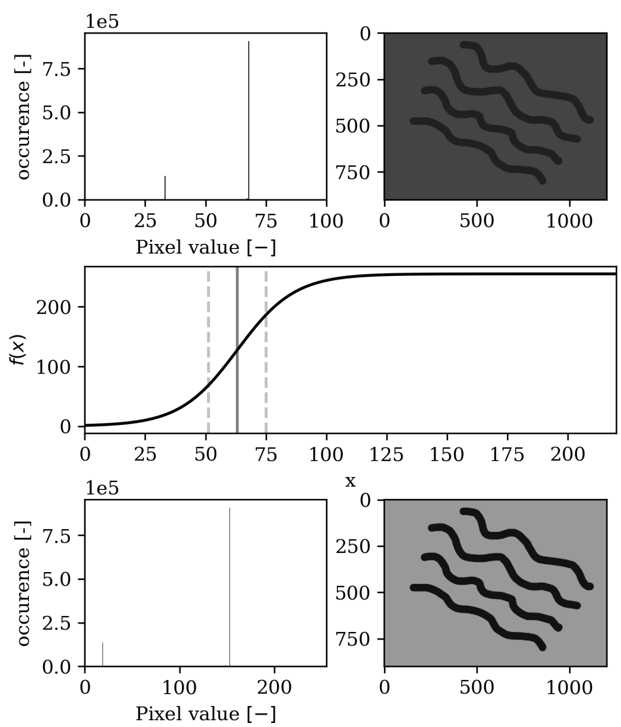

Figure 5: The example figure modified using a sigmoid function.

In figure 5 on the left, the low contrast example figure and its histogram are plotted in the top row. In the middle row a sigmoid function has been plotted, as well as the median value and the standard deviation of the histogram above denoted by respectively the grey solid and grey dashed line. The bottom row consists of the histogram of the example image and the image acted on by the sigmoid function. In this example we used a sigmoid function $f'(x) = f(x) \cdot 255$ since we want to map our input values on a domain $[0, 255]$ not $[0, 1]$, α is the median of the top histogram and β its standard deviation.
As can be seen in the figure the peaks of the most common values of the intensity have been spread further apart thus resulting in a higher contrast image.

Rank filters are a type of linear filters that make use of the local grey scale pixel values. This type of filter first makes a grey scale histogram of the pixels in the neighbourhood of the to-be-altered pixel to apply a local filter for smoothing, sharpening, noise reduction etc. ([8]).
For this experiment, the bilateral mean filter, $BILAT$, the local contrast enhancement filter, $CONT$, and the local morphological contrast enhancement filter, $MORPH$, are implemented on the image

of the fungus using the python Scikit-image package.
$BILAT$ makes the grey-level of pixels in a local neighbourhood similar to the central ones. It should therefore help to reduce noise. $CONT$ improves contrast for every local neighbourhood. $MORPH$ replaces a pixel values for either the local maximum or the local minimum. ([8])
The image that is being used for this part of the experiment is zoomed-in in order to see noise and fine details. A radius of $r_{local} = 20$ is used for $BILAT$, and for the other filters, a radius of $r_{local} = 5$ pixels is used for the local pixel neighbourhood. To explore how the image can be improved best, the filters are used in different combinations and compared.

4 Results and discussion

4.1 Calibration

The values that have been found for $d_{physical}$, n_{pixels}, l_{pixel} and the corresponding error are presented in table 1 for each objective. It was estimated that $u(n) = 4$. The images corresponding to each measurement are presented in figures 14, 15 and 16 in appendix Appendix B.

Table 1: Results of measurements of n_{pixels} for the corresponding value of $d_{physical}$ for each objective. The values for l_{pixel} and $u(l_{pixel})$ follow from respectfully equation 1 and 5.

Objective	$d_{physical}$ $(m) \cdot 10^{-3}$	n_{pixels}	l_{pixel} (m)	$u(l_{pixel})$ (m)
4×	1	$6.85{\cdot}10^{2}$	$1.461{\cdot}10^{-6}$	$9{\cdot}10^{-9}$
10×	0.8	$1.247{\cdot}10^{3}$	$6.42{\cdot}10^{-7}$	$2{\cdot}10^{-9}$
40×	0.2	$1.250{\cdot}10^{3}$	$1.600{\cdot}10^{-7}$	$5{\cdot}10^{-10}$

As expected, the accuracy for the higher magnification objectives is better. Meaning that images from an objective with a higher magnification, corresponds with a smaller value for l_{pixel}.

4.2 Resolving power

The photos below are the result of the process outlined in the section 3.1. The high an low values of the line trace were manually read from the images and entered into a python script to calculating the visibility values for each magnification and spatial frequency. The result of which can be seen in figure 8.

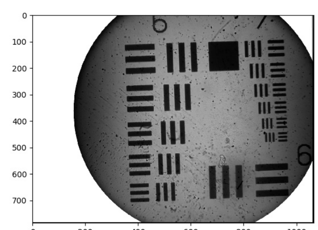

Figure 6: Gray-scale image of resolution target with 40× objective. The numbers on the axes correspond to the pixel count.

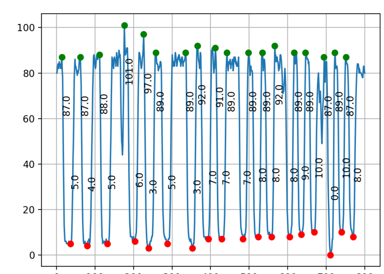

Figure 7: Linetrace of seventh group.

The above photos are the result of the process outlined in the section 3.1. The high an low values of the line trace were manually read from the images and entered into a python script to calculating the visibility values for each magnification and spatial frequency. The result of which can be seen in figure 8.
The data is plotted in such a way that the highest subplot has the lowest magnification and the lowest subplot has the highest magnification. Each subplot has the dimensionless visibility number plotted on the vertical axis and the spatial frequency plotted on the horizontal axis. We chose this layout since we expect the visibility to decrease when the lines get closer together and the spatial frequency consequently increases. Note that only the vertical visibility axis of the highest sub-plot starts with a visibility of zero.
What we see is not surprising when we also take into account the photos in the appendix. As can be seen on these photos the 40× objective has the smallest numerical aperture, therefore all three traced groups are clearly resolvable. Thus, the visibility won't drop as much for the 4× objective when the spatial frequency increases.

Something noticeable however, is that the highest magnification plot starts of with the lowest visibility value. This has to do with the fact that this smaller aperture also catches less light, the brightest spot in its photo is evidently less bright than that of the other two apertures. This can be seen when taking a look at either the line-traces or the photos in the appendix.

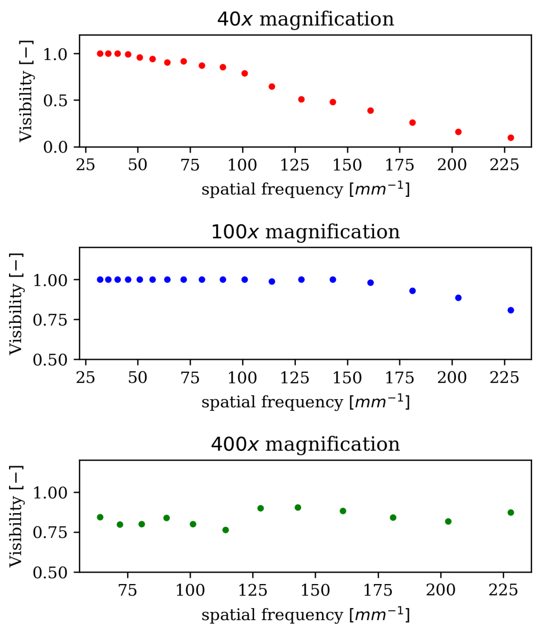

Figure 8: Plots of the visibilities per numerical aperature.

4.3 Size measurements

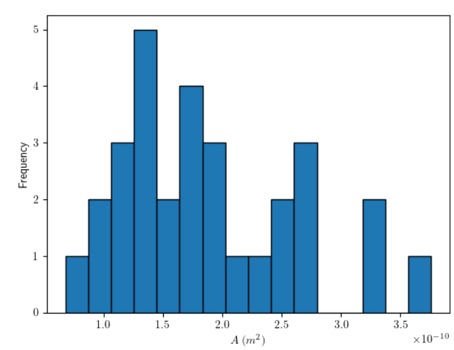

Figure 9: Histogram of the values of A for 30 starch particles.

From the data and equations 1 and 5, it follows that the values of d_{hair} and d_{gf} are respectively $d_{hair} = 6.57 \pm 0.08 \cdot 10^{-5} m$ and $d_{gf} = 1.26 \pm 0.01 \cdot 10^{-4} m$. The images used for the measurements are presented in Appendix C.
The errors of the values for d_{hair} and d_{gf} are in the order of 1 %. Furthermore, the values for d_{hair} and d_{gf} are of expected magnitude.
The values for a, b, A, the corresponding errors and the corresponding images that have been used can be found in Appendix C. A histogram of the values for A is presented in figure 9.
The values for A are in the right order of magnitude ([2]) and have an error of under 5 %. A mean value of $A = 1.9 \cdot 10^{-10}\ m^2$ with a standard deviation of $\sigma = 8 \cdot 10^{-11}\ m^2$ follows from calculation. The histogram shows that the distribution is not symmetrical with relatively many outliers for large values of A. This result cannot be generalised for all starch particles since only ellipse-shaped particles were taken into account. Reviewing the images that were used for the analysis (see Appendix C) reveals that there are relatively many large starch particles that are not ellipse shaped and therefore not taken into account. Furthermore, it was only possible to get unambiguous ellipse fits for a relatively small number of particles. Most of the particles were not clearly visible or not of the right shape. Therefore, this method did not prove to be sufficient for this type of particle measurements. Other microscopy techniques, in combination with automated blob finding algorithms could possibly be of

better use.

4.4 Birefringence

The colour planes that were taken into account for this experiment can be seen in figure 10 in which each Roman numeral corresponds to a colour plane.
The values that have been found for f, Δl_{path}, D and the corresponding errors are presented in appendix Appendix D.
In figure 11, Δl_{path} is plotted as a function of D. The data point corresponding to plane IV, the one with the cross, was not taken into account to find Δn. The reason for this, given the distance of this data point compared to the best fit, is that it seems that an error was made during the experiment. This error could be the result of inadequate focussing on colour planes. The reason for this being the ambiguity of what details to focus on for each colour plane.
It follows from the orthogonal distance regression that $\Delta n = 5.3 \pm 0.2 \cdot 10^{-2}$. According to the Michel-Lévy chart from [4], the sample could either be astrophylite, silk or piemontite.
The method that was used seemed to give a relatively precise outcome - only giving three possible sample materials. However, given that it is not clear why the value for colour plane IV is an outsider, one could argue the validity of the outcome.
To find out if this experimental set-up is sufficient, the found value for Δn should be compared to the theoretical value for the sample. This theoretical value, is however not available.

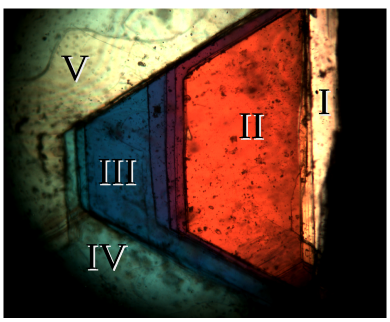

Figure 10: Image of a birefringent crystal in a polarizing microscope. The Roman numerals correspond to the different colour planes that were taken into account for this experiment.

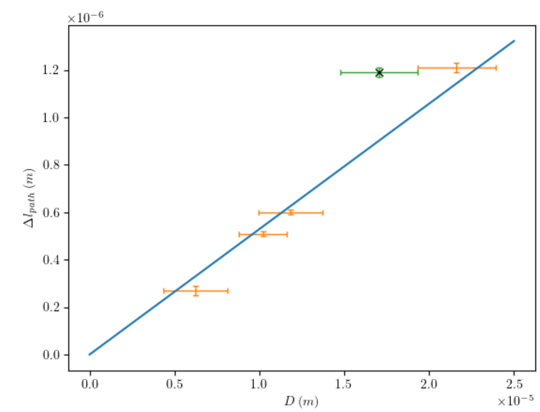

Figure 11: Δl_{path} plotted as a function of D. The data points have errorbars in Δl_{path} and D. The straight line is a best fit to the data according to an orthogonal distance regression using equation 3. The data point with the cross was not taken into account to find Δn.

4.5 Image improvements methods

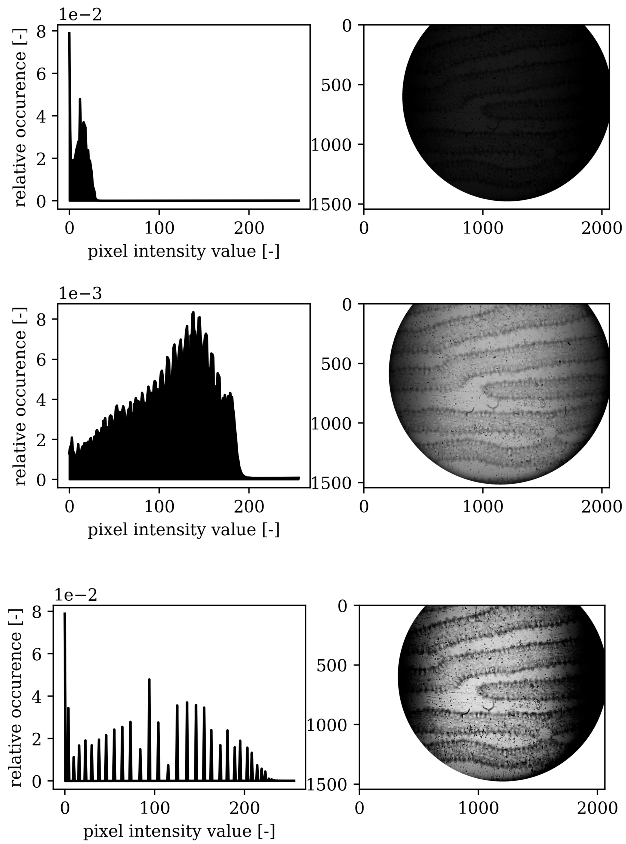

Figure 12: Images of fungus sample with 40× objective and corresponding intensity plot. From top to bottom: an underexposed image, an auto exposed image and the underexposed image altered by a sigmoid. The numbers on the axes of the image correspond to the pixel count.

The two topmost pictures in figure 12 are images of the fungus sample using the same camera with different exposure settings. As can be seen the top image is clearly underexposed as the peaks of its histogram lie solely in the lowest quarter of the intensity spectrum. The second topmost image was taken at an auto-exposure setting meaning that the camera itself decides the best exposure setting. The bottommost picture contains the same information as the underexposed top image, the information however is spread over the total intensity spectrum by a sigmoid function as explained in 3.4. The peaks of the improved image's histogram still represent the histogram of the top image.
Since information cannot be added to the image, the bottommost image is only better when looked at it by a person, the histogram is discontinuous meaning that there is not as much transition between two values. This is especially noticeable at the edges of the frame where the original image is so dark that there is no information to spread. Since there are only one or two intensity values the resulting shift will still only consist of two values, resulting in shifted black bars.
Because of the previous reason it would be safe to assume that the algorithm used could greatly improve if some sort of interpolation function is also added. This way the program would be able to try and fill in missing information.

A close-up of the original image of the fungus with the 40× objective and close-ups of the images that were acquired using the *BILAT*,*CONT* and *MORPH* rank filters in different combinations are presented in figure 13. The image is zoomed-in in order to see the filtering effects thoroughly. The zoomed-in image seems to be out of focus. This is caused by a limited resolving power of the microscope compared to the fine details of the fungus sample.
As expected, the *BILAT* filter filters away some of the noise. This can be seen by the reduction of small dots in figure 13b. However, it also removes some of the details. The *CONT* filter improves contrast efficiently, making details more visible A downsides of the filter is, however, that it emphasizes noise and the dark edges. This causes the edges to lose quality. This could perhaps be solved by first using a high-pass filter to remove the slow darkening transition towards the edges. The *MORPH* filter makes the edges between different components in the image more clearly visible. Which could prove to be useful when doing size measurements within the image or when imposing edge detecting. What's more, it also seems to reveal more of the details. A negative artefact of the

$MORPH$ filter is that it emphasizes noise.
Combining the filters also proves to be useful, especially combinations with the $BILAT$ filter. In this case, the noise removal and detail loss is compensated by either of the other two filters (see figure 13g and 13e). However, when many details need to be revolved, one might be better-off not using the $BILAT$ filter and accepting relatively much noise (see figure 13f).

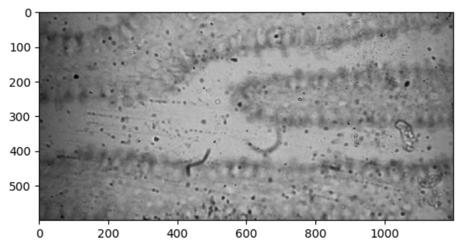

(a) Zoomed-in gray-scale image of sample.

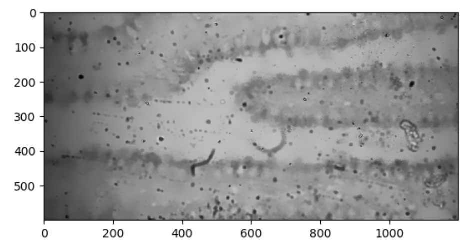

(b) Image using $BILAT$, $r_{local} = 20$ pixels.

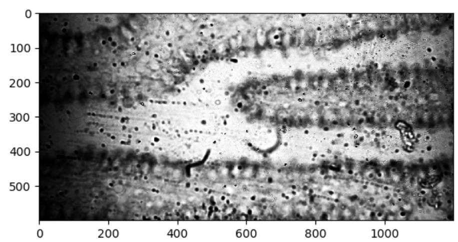

(c) Image using $CONT$, $r_{local} = 5$ pixels.

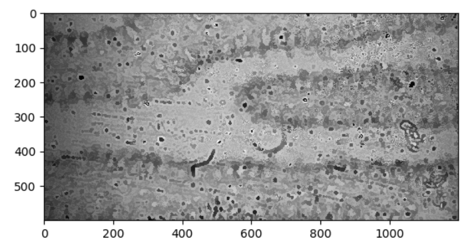

(d) Image using $MORPH$, $r_{local} = 5$ pixels.

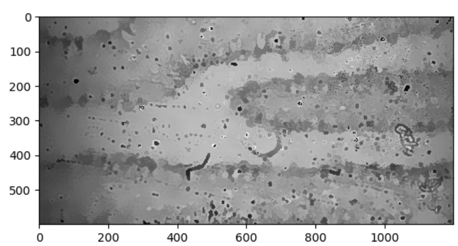

(e) Image using respectively $BILAT$ and $MORPH$.

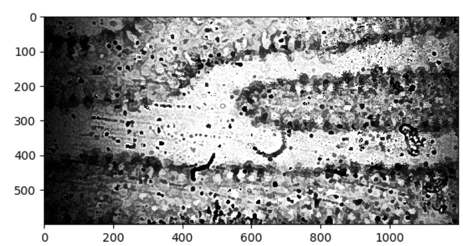

(f) Image using respectively $CONT$ and $MORPH$.

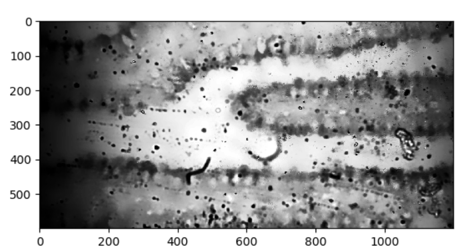

(g) Image using respectively $BILAT$ and $CONT$.

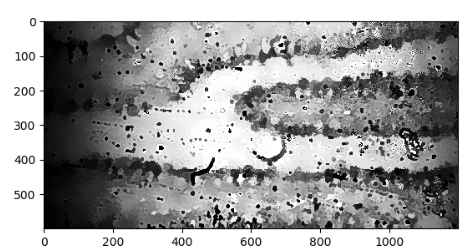

(h) Image using respectively $BILAT$, $CONT$ and $MORPH$.

Figure 13: Set of images of fungus sample using the $BILAT$,$CONT$ and $MORPH$ rank filters in different combinations. The images were acquired using the $40\times$ objective and are zoomed-in, in order to see fine details. The numbers on the axes correspond to pixel counts.

5 Conclusions

The values that were found for the length corresponding to a pixel l_{pixel} to be $1.5 \cdot 10^{-6}$, $6.4 \cdot 10^{-7}$ and $1.6 \cdot 10^{-7}$ for the $4\times$, $10\times$ and $40\times$ objectives respectively. This was easily achieved with the aid of the NI Vision software.
The results for the visibility for the objectives were as expected apart from the fact that the highest magnification objective had a lower visibility starting point, this however was explained by the fact that this object had an overall lower intensity image because its low numerical aperture meant it caught less light. The NI Vision also proved to be helpful with determining the resolving power of the multiple magnification objects by being able to export a line trace of the pixel intensity.
The values that was found for the diameter of a human hair and glass fibre are respectively $d_{hair} = 6.57 \pm 0.08 \cdot 10^{-5} m$ and $d_{gf} = 1.26 \pm 0.01 \cdot 10^{-4} m$. For the starch particles a mean value of $A = 1.9 \cdot 10^{-10} m^2$ with a standard deviation of $\sigma = 8 \cdot 10^{-11}\ m^2$ was found for the cross section. The size measurements yielded results that matched literature. However, the measurements on the starch particles turned out to be inadequate given the shape and number of unresolvable particles.
The value that was found for the birefringence of the crystal is $\Delta n = 5.3 \pm 0.2 \cdot 10^{-2}$. Therefore, the crystal could either be astrophylite, silk or piemontite. Given that there is an unidentified measurement error, the validity of the outcome is debatable.
Improving the image using the sigmoid function and a contrast enhancing rank filter works well, significantly improving the contrast of the image. A bilateral mean filter proves to be of use when removing noise. It does however, remove some of the details. A morphological contrast enhancement filter can be useful for size measurements or line detection. Combination of the different rank filters also seems to be useful to either reveal much detail or to remove noise, compensated by gain of contrast.

References

[1] E. Hecht, *Optics.* Pearson Education, Inc., 2016.

[2] H. Saari, K. Heravifar, M. Rayner, M. Wahlgren, and M. Sjöö, "Preparation and characterization of starch particles for use in pickering emulsions," *Cereal Chemistry*, vol. 93, no. 2, pp. 116–124, 2016.

[3] M. Abramowitz and M. W. Davidson, "Optical birefringence." `http://olympus.magnet.fsu.edu/primer/lightandcolor/birefringence.html`, 2012.

[4] C. Zeiss, "Michel-lévy color chart." `https://applications.zeiss.com/C125792900358A3F/0/E037A9841E664961C1257906004802D6/$FILE/70_2_0110_e_michel_levy.pdf`.

[5] "Image processing with ni vision development module." `https://www.ni.com/nl-nl/innovations/white-papers/06/image-processing-with-ni-vision-development-module.html`, mar 2019.

[6] T. Wilson, M. Friedrich, and A. Diaspro, *Basics of light microscopy and imaging.* Olympus.

[7] D. S. Lal and M. Chandra, "Efficient algorithm for contrast enhancement of natural images," *International Arab Journal of Information Technology*, vol. 11, pp. 96–102, 01 2014.

[8] "Rank filters." `https://scikit-image.org/docs/0.12.x/auto_examples/xx_applications/plot_rank_filters.html`.

Appendix A Leica DM EP manual

Leica DM EP

The Microscope for Teaching and Research

- **Advanced performance in a teaching polarizing microscope:**
  - Standard and advanced conoscopy modules
  - Polarizer with notch markings
  - 4-position objective turret, centerable
  - Sturdy, compact design
- **Convenience that makes work easy:**
  - Easy-to-access control functions
  - Ergonomic viewing angle
  - Accurate angular measurement with verniers on the rotating stage

Developed for college teaching and research use:
the Leica DM EP.

Accurate and versatile for teaching
The Leica DM EP is the ideal polarizing microscope for university and other instructional use, offering a standard and an advanced Bertrand lens module for unsurpassed ease of operation. With a wide range of accessories and Leica's renowned optics, the Leica DM EP is exceptional not only for its compact, durable design, but also for its efficiency and ease of operation.

Designed for optical brilliance and long life illumination
The standard Köhler field diaphragm and magnetically fixed blue filter provide vivid, pin-sharp images. The 2,000-hour, 35-watt halogen lamp saves hundreds of dollars in replacement bulb cost over the life of the microscope. An illuminated intensity control system reminds the user to switch off the lamp after finishing work to increase the lamp's service life and save energy.

Maximum ease of use and high optical brilliance are
the outstanding features of the Leica DM EP.

Modular, Customized Configurations – Microscopes Designed for You

- **Flexibility that gives the freedom you need:**
  – Wide selection of POL objectives

- **Compatibility that knows no bounds:**
  – Fully compatible components across Leica's polarizing microscope product line
  – Wide selection of analyzers, polarizers, and compensators
  – Full wave & quarter wave plates are available
  – Wide selection of POL observation tubes

The result of combining maximum precision and optimum ergonomic design – the 360° analyzer.

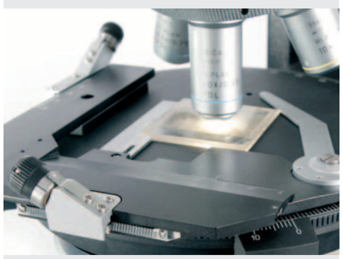

Flexibility is key. All of Leica's rotating stage polarizing microscopes feature attachable, interchangeable mechanical stages.

Flexibility – Designed for you

Flexible to the last detail. All Leica polarizing microscope components can be configured for all microscopes in the polarizing line. For example, you can choose from over twenty POL objectives for the Leica DM4500 P, DM2500 P or DM EP. The optical possibilities are unlimited. You will enjoy the benefits provided by this complete system when using the new 360° analyzer, the 360° polarizer or even with full wave plates. All components can be used for classroom teaching, everyday routine work, and research.

Leica's entire line of DIN standard compensators can be used in all Leica polarizing microscopes, as can the attachable mechanical stage for accurate sample positioning. This always ensures flexible interchange and replacement of parts.

Technical Data

	Leica DM EP	Leica DM2500 P	Leica DM4500 P
• **Objective turret**	4x (M25), centerable	5x (M25), centerable	6x (M25), centerable, absolute encoded
• **Objectives**	HI Plan POL N Plan POL Immersion objectives	HI Plan POL N Plan POL PL Fluotar POL Immersion objectives	HI Plan POL N Plan POL PL Fluotar POL Immersion objectives
• **Usable field of view**	20 mm	25 mm	25 mm
• **Contrast method** **Changeover** **Color reproduction** **Transmitted light** **Incident light**	 Manual Polarization contrast Orthoscopy Conoscopy Brightfield Phase contrast Darkfield Polarization contrast Brightfield	 Manual Polarization contrast Orthoscopy Conoscopy Brightfield Phase contrast DIC Darkfield Polarization contrast Brightfield Darkfield* DIC Fluorescence	 Motorized CCIC: Constant Color Intensity Control Polarization contrast Orthoscopy Conoscopy Brightfield Phase contrast DIC Darkfield Polarization contrast Brightfield Darkfield* DIC Fluorescence
• **Conoscopy**	Bertrand lens cube in new IL axis Bertrand lens module (AB module) Advanced conoscopy module	Bertrand lens cube Bertrand lens module (AB module) Advanced conoscopy module	Fully integrated conoscopy beam path User guidance with display feedback
• **Transmitted light axis** **Illumination** **Operation**	 12 V 35 W halogen lamp Manual User guidance with CDA	 12 V 100 W halogen lamp Manual User guidance with CDA	 12 V 100 W halogen lamp Motorized Integrated illumination manager
• **Incident light axis**	Manual User guidance with CDA	Manual User guidance with CDA	Motorized Integrated illumination manager, round and rectangular field diaphragms for ocular or camera observation
• **Condensers**	Manual changeover User guidance with CDA	Manual changeover User guidance with CDA	Motorized changeover of condenser head, 7x condenser disc, polarizer
• **Focus drive**	Manual, 2-gear gearbox	Manual, height-adjustable, Focus stop, 2 or 3-gear gearbox	Manual, 2-gear gearbox

* on request

Appendix B Calibration

The three images that are used to find l_{pixel} for each objective can be found in figure 14, 15 and 16. The numbers on the axes correspond to the pixel count.

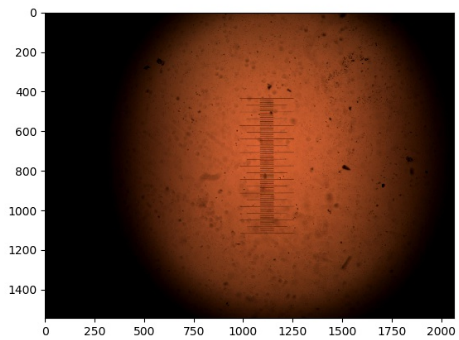

Figure 14: Image used to find l_{pixel} for the 4× objective.

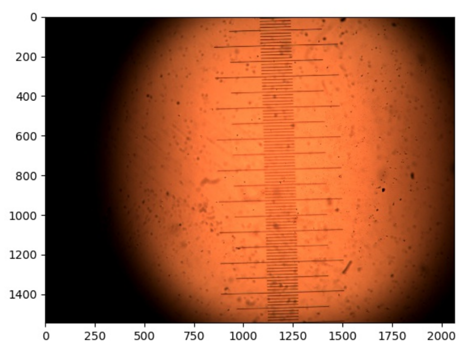

Figure 15: Image used to find l_{pixel} for the 10× objective.

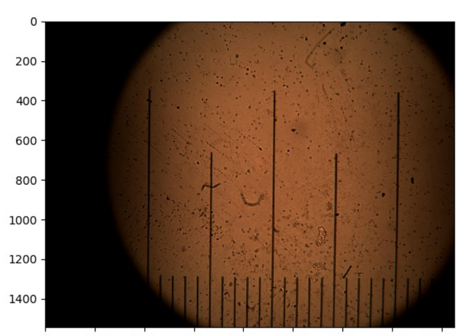

Figure 16: Image used to find l_{pixel} for the 40× objective.

Appendix C Size Measurements

The images used to find d_{hair} and d_{gf} are presented in respectively figure 17 and 18. The numbers on the axes correspond to the pixel count.

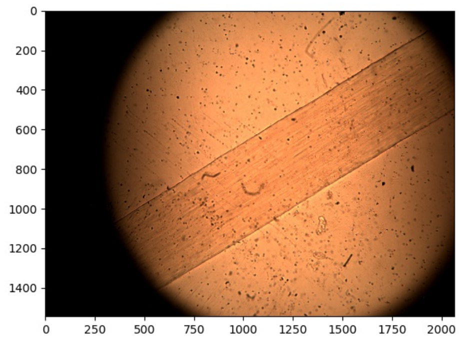

Figure 17: Image used to find d_{hair}.

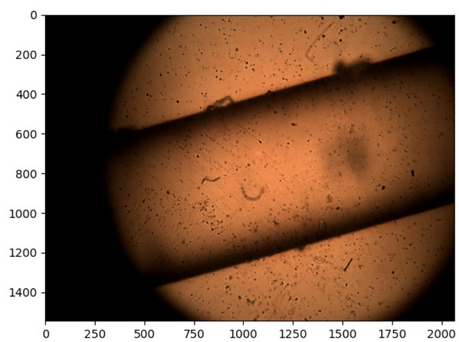

Figure 18: Image used to find d_{gf}.

The values that have been found for a, b, A and the corresponding errors are presented in table 2.

Table 2: Results of measurements of a and b for 30 starch particles. It was estimated that $u(a) = u(b) = 2\,pixels$. The values for A and $u(A)$ follow from equations 1, 5, 2 and 6. The particles corresponding to each number can be seen in figures 19a to 19f.

Particle number	$a\ (\#pixels)$	$b\ (\#pixels)$	$A \cdot 10^{-10}\ (m^2)$	$u(A) \cdot 10^{-12}\ (m^2)$
1	84	76	1.28	5
2	83	75	1.25	5
3	85	77	1.32	5
4	72	67	0.97	4
5	97	94	1.83	6
6	58	58	0.68	3
7	70	66	0.93	4
8	105	95	2.01	6
9	92	90	1.67	5
10	84	82	1.39	5
11	115	115	2.66	7
12	146	128	3.76	8
13	119	110	2.63	7
14	76	75	1.15	4
15	112	108	2.43	6
16	127	125	3.19	7
17	99	90	1.79	6
18	84	81	1.37	5
19	135	123	3.34	8
20	80	78	1.26	5
21	86	84	1.45	5
22	112	106	2.39	6
23	105	103	2.18	6
24	74	72	1.07	4
25	117	116	2.73	7
26	90	83	1.50	5
27	100	91	1.83	6
28	117	104	2.45	6
29	100	97	1.95	6
30	99	92	1.83	6

The images that were used to find the data in table 2 can been seen in figure 19

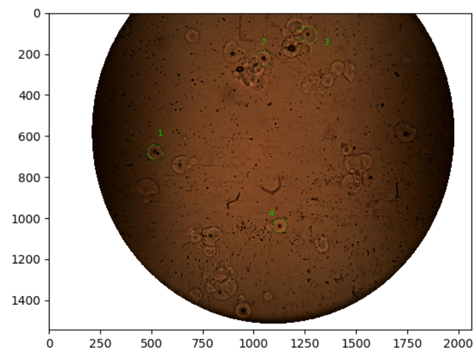

(a) Best ellipse fits for starch particles 1 to 4.

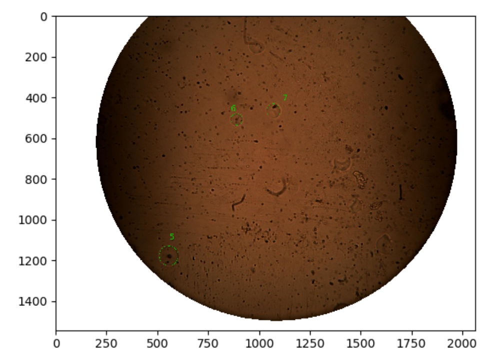

(b) Best ellipse fits for starch particles 5 to 7.

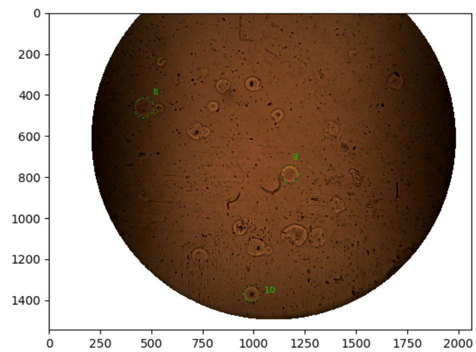

(c) Best ellipse fits for starch particles 8 to 10.

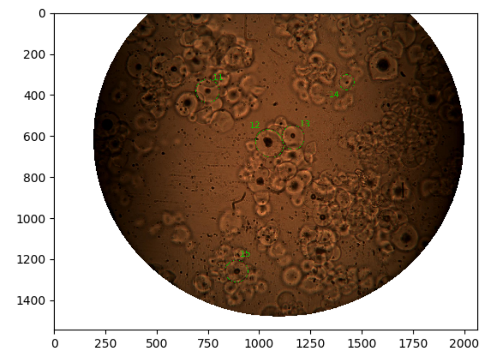

(d) Best ellipse fits for starch particles 11 to 15.

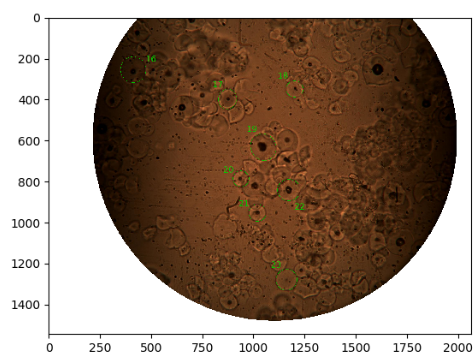

(e) Best ellipse fits for starch particles 16 to 23.

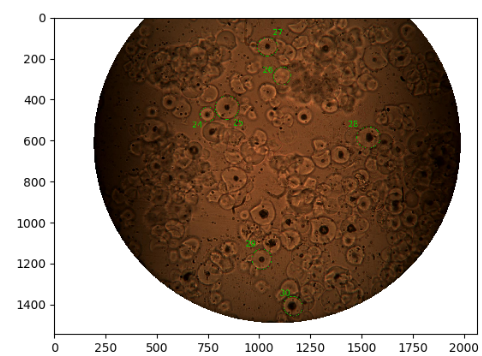

(f) Best ellipse fits for starch particles 24 to 30.

Figure 19: Set of images used to find best ellipse fits for 30 starch particles. The green ellipses represent the best fit. The numbers on the axes, correspond to the pixel count.

Appendix D Birefringence

The results for f for each colour plane is presented in table 3. It was estimated that $u(f) = 2 \cdot 10^{-6}$ (m).

Table 3: Results of measurements of f. The Roman numerals represent the different colour planes (see figure 10). The letters A, B, C and D represent different measurements at different locations of the sample.

A		B			C		D	
$f_{bottom} \cdot 10^{-5}$ (m)	$f_{II} \cdot 10^{-5}$ (m)	$f_{II} \cdot 10^{-5}$ (m)	$f_{III} \cdot 10^{-5}$ (m)	$f_{V} \cdot 10^{-5}$ (m)	$f_{III} \cdot 10^{-5}$ (m)	$f_{IV} \cdot 10^{-5}$ (m)	$f_{I} \cdot 10^{-5}$ (m)	$f_{II} \cdot 10^{-5}$ (m)
1.5	2.5	2.2	2.4	3.3	7.0	6.5	6.0	6.4
1.4	2.5	2.3	2.4	3.5	7.1	6.5	6.0	6.5
1.5	2.5	2.3	2.5	3.7	7.0	6.5	6.1	6.5
1.6	2.5	2.4	2.6	3.7	3.0	6.5	6.1	6.4
		2.6	2.8	3.4	7.1	6.6	6.0	6.5

The values for D follow from the values of f. The values for D, Δl_{path} and the corresponding errors are presented in table 4.

Table 4: Results for measurements of D, Δl_{path} and the corresponding errors for each colour plane (see figure 10). The values of D were found with simple addition and subtraction using the values of f. The values of Δl_{path} were found using a Michel-Lévy birefringence chart ([4]).

Colour Plane	$D \cdot 10^{-5}$ (m)	$u(D) \cdot 10^{-6}$ (m)	$\Delta l_{path} \cdot 10^{-7}$ (m)	$u(\Delta l_{path}) \cdot 10^{-8}$ (m)
I	0.6	2	2.7	2
II	1.0	1	5.1	1
III	1.2	2	6.0	1
IV	1.7	2	11.9	2
V	2.2	2	12.1	2